Low Loss CMOS-Compatible PECVD Silicon Nitride Waveguides and Grating Couplers for Blue Light Optogenetic Applications
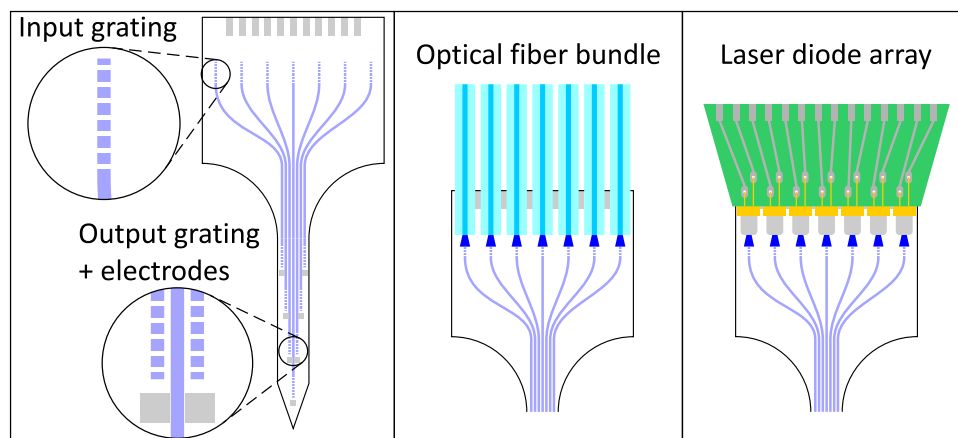
Luis Hoffman, *Member, IEEE*
Ananth Subramanian
Philippe Helin
Bert Du Bois
Roel Baets, *Fellow, IEEE*
Pol Van Dorpe
Georges Gielen, *Fellow, IEEE*
Robert Puers, *Fellow, IEEE*
Dries Braeken

Low Loss CMOS-Compatible PECVD Silicon Nitride Waveguides and Grating Couplers for Blue Light Optogenetic Applications

Luis Hoffman,[1,2] *Member, IEEE*, **Ananth Subramanian,**[3,4]
Philippe Helin,[1] **Bert Du Bois,**[1] **Roel Baets,**[3,4] *Fellow, IEEE*,
Pol Van Dorpe,[1,5] **Georges Gielen,**[2] *Fellow, IEEE*,
Robert Puers,[2] *Fellow, IEEE*, and **Dries Braeken**[1]

[1]Imec, Leuven 3001, Belgium
[2]Electrical Engineering Department (ESAT), KULeuven, Leuven 3001, Belgium
[3]Photonics Research Group, iGent—Universiteit Gent, Gent 9052, Belgium
[4]Department of Information Technology, Center for Nano and Biophotonics, Gent 9052, Belgium
[5]Department of Physics, KULeuven, Leuven 3001, Belgium

Abstract: This paper presents silicon nitride (Si_xN_y) photonic integrated circuits (PICs) with high performance at a wavelength of 450 nm, which, therefore, is suitable for neuronal stimulation with optogenetics. These PICs consist of straight and bent waveguides, and grating couplers that are fabricated in a complementary metal-oxide-semiconductor (CMOS)-compatible plasma enhanced chemical vapor deposition Si_xN_y platform. Their characterization shows propagation losses of 0.96 ± 0.4 dB/cm on average for straight waveguides that are 1–5 μm wide and bend insertion losses as low as 0.2 dB/90° for 1 μm wide waveguides with a radius of 100 μm. Additionally, the grating coupler characterization shows that they can deliver about 10 μW of light in an area of 5×9 μm^2 (240 mW/mm²), which is captured from an uncollimated laser diode (70 mW). Besides delivering sufficient power for optogenetic applications, the gratings have dimensions that are comparable to the size of a neuron, which would allow single cell interaction. These results demonstrate that, with this Si_xN_y platform, high-density and large-scale implantable neural devices can be fabricated and readily integrated into existing CMOS-compatible neuro-electronic platforms.

Index Terms: Gratings, fabrication and characterization, waveguide devices, light-tissue interactions

1. Introduction

Silicon nitride (Si_xN_y) has become a very popular platform for the development of biophotonic devices. To start, Si_xN_y is not only transparent for infrared but also for the visible range down to the blue color [1]. Moreover, its refractive index (n $\sim$ 2) is well balanced: on the one hand, it is higher than other popular transparent waveguide materials like glasses (n $\sim$ 1.45 – 1.5), SU-8 (n $\sim$ 1.6
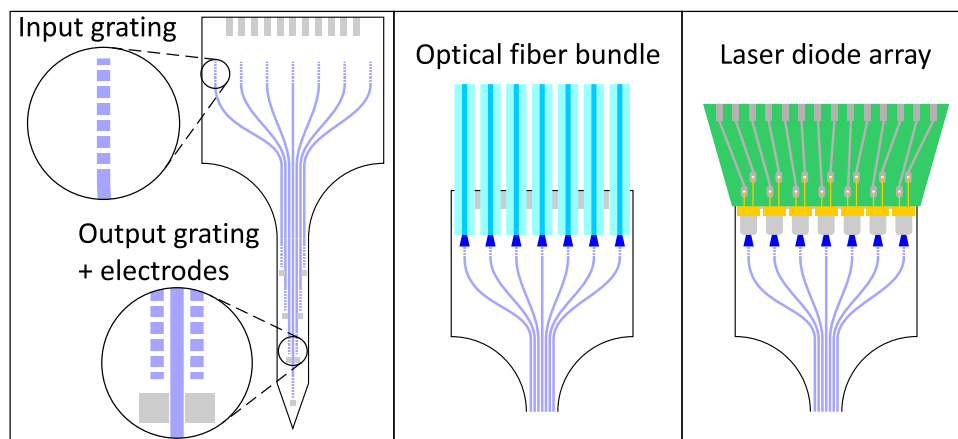
Fig. 1. Conceptual design of an implantable device for *in vivo* optogenetics. The non-implantable part of the device has an array of grating couplers that are used to couple light in from an external source. The waveguides then transport the light into the implantable shank. In this section of the device, there is another set of grating couplers that expel the light nearly perpendicular out of the waveguides and towards the tissue. Recording electrodes are placed in the vicinity of each out-coupler. Either a bundle of optical fibers or an array of laser diodes could be used as a light source for the system.

[2]) and silicon oxynitride (n $\sim$ 1.5 [3]), which allows for tighter light confinement in the core and therefore, for denser integration. On the other hand, it is not as high as silicon in SOI (n $\sim$ 4.7 at 450 nm [4]) which makes Si_xN_y devices less sensitive to processing defects and scattering losses [5]. The latter is particularly important to fabricate high quality devices. Finally, the possibility to fabricate devices with complementary metal-oxide-semiconductor (CMOS) compatible processes [6], [7] makes the products reproducible, scalable and suitable for monolithic integration with active electronic components.

Optogenetics is a technique that uses light to control "well-defined events within any specific cell of living tissue" [8]. The targeted cells (i.e. neurons) become light-sensitive by incorporating light-controlled channels, so called opsins, into them. Since the absorption peak of Channelrhodopsin-2, a widely used opsin, is at 480 nm [9], an optogenetic device should work within the blue-light range (i.e. wavelength range from 450 nm to 495 nm). Moreover, as optogenetics is commonly used in mice for chronic *in vivo* experiments, the device should also be lightweight, small and free of complicated tethers. It should also incorporate a large number of excitation sites, which should be comparable to the size of a neuron, as this allows their individual manipulation, and therefore, increases the degrees of freedom for neuroscientific experimental design. All these challenges can be addressed by devices fabricated with a Si_xN_y photonic platform. Fig. 1 presents a conceptual design that shows how Si_xN_y waveguides and grating couplers can be used to fabricate an implatable device for *in vivo* optogenetic stimulation.

Manufacturing photonic integrated circuits (PICs) that work at lower wavelengths (blue and UV) is particularly challenging because at these wavelengths material absorption increases (Tauc's law [10]), scattering due to wall roughness increases ($\propto 1/\lambda^4$) and smaller feature sizes are required, especially for single mode waveguides. Despite these challenges, there are recent examples of optogenetic devices that use Si_xN_y waveguides [11]–[14]. However, the first two were fabricated with Si_xN_y that was deposited with low pressure chemical vapor deposition (LPCVD), which is a high temperature process, and therefore difficult to combine with other processes like CMOS circuitry or metalization layers.

Furthermore, none of these publications presented a complete characterization of the performance of the material and waveguide technology for blue light, which is important to understand the limitations and capabilities of the technology. This work aims to close this gap by the design and characterization of PICs at 450 nm (suitable for optogenetic stimulation) built on a CMOS-compatible Plasma Enhanced Chemical Vapor Deposition (PECVD) Si_xN_y platform which uses 193 nm optical

lithography. The designed PICs consist of rectangular waveguides, waveguide bends and grating couplers. The results obtained in the present work demonstrate that the presented Si_xN_y platform performs well at 450 nm and is well-suited for single cell resolution. Moreover, they increase the understanding of how far this technology can be pushed for the fabrication of highly integrated optogenetic devices.

2. Design and fabrication

2.1 Waveguide Design

The size constraints for optogenetic implantable devices permit using only simple light sources, normally, with no intermediate optics, and with divergent emission. Light with these characteristics is more efficiently coupled into wide waveguides. However, narrow waveguides are required because they allow for narrower implants with a larger amount of optical outputs. Therefore, a trade-off has to be found, and this is accomplished with test waveguides of different widths.

The maximum test width can be established based on the knowledge that a typical silicon brain implant has a width around 100 μm (for instance, see [15] and [16]). Moreover, this width could accommodate about sixteen 5 μm wide waveguides, and therefore optical outputs. Less than this would not be desirable. Thus, 5 μm was set as the maximum width for the test structures. The minimum test width can be defined so that the total number of propagating modes remains sufficiently large. For a given width, the amount of propagating modes depends on the core's height, which can be selected with the slab waveguide cut-off height for the traverse electric (TE) modes. This parameter is given by the following expression [17, p. 27]:

$$h_{cut-off} = \frac{\lambda_0}{2\sqrt{n_{core}^2 - n_{clad}^2}} \tag{1}$$

where n_{core} and n_{clad} are the refractive index of the core (1.92) and the refractive index of the cladding (1.46), respectively [6], and λ_0 is the free space wavelength (450 nm). With these values, equation (1) results in a cut-off height of 180.0 nm, which was selected as height. Subsequently, determining the minimum width required calculating the dispersion diagrams for the rectangular waveguide with respect to the width and height (see Fig. 2). The diagrams were obtained with a simulation of the waveguide with COMSOL's 2D mode solver and its electromagnetic waves frequency domain (ewfd) physics interface. This simulation showed that at a width of 1 μm the number of modes are only four for both quasi-traverse electric (TE) and quasi-traverse magnetic (TM) polarizations [see Fig. 2(b) and (d)] and that for the narrower widths, the quantity of modes diminishes rapidly. The power captured from a divergent source would follow the same trend, and therefore, the lower limit of the test range was set to 1 μm. Finally, the dispersion diagram with respect to the height for a width of 5 μm [see Fig. 2(a) and (c)] confirms that the waveguides would have only one vertical mode for the proposed range of heights.

2.2 Grating Coupler Design

Grating couplers are used to directly and efficiently couple light, typically from optical fibers, into PICs [18]. Fig. 3 shows the basic grating coupler design parameters. First, the fill factor (d_{groove}/Λ) was set to 0.5, which normally results in a better fabrication tolerance [7] and coupling efficiency [19]. Secondly, the grating coupler period (Λ) was set to 300 nm, which was the smallest period (grooves 150 nm wide) that could reliably be fabricated with the available 193 nm lithography. For this grating coupler period, the methodology proposed in [20] predicts an in/out-coupling angle (Θ) into Si_xO_y of around 10°.

The last grating parameter to determine is the depth of the grating coupler groove (h_{groove}) which is used for the optimization of the in/out-coupling efficiency and emission size. For telecommunication applications, grating couplers are normally optimized to interact with single mode optical fibers. In this situation, the beam profile emitted by the grating coupler should closely match the mode profile
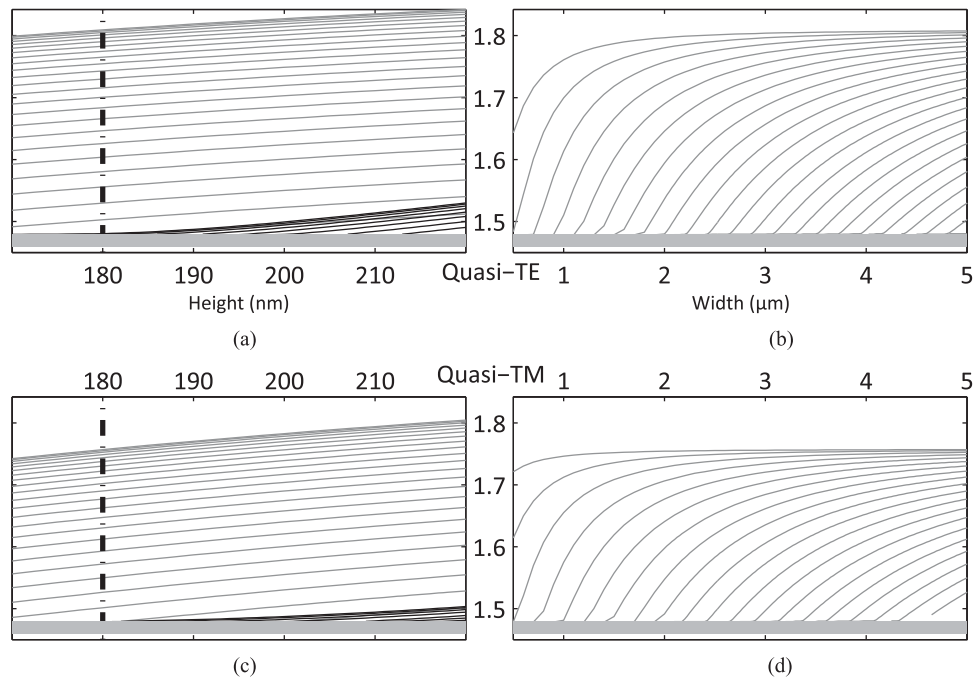
Fig. 2. Dispersion diagrams: Neff variation with respect to waveguide width and height. (a) Quasi-TE modes with respect to height at 5 μm width. (b) Quasi-TE modes with respect to width at 180 nm height. (c) Quasi-TM modes with respect to height at 5 μm width. (d) Quasi-TM modes with respect to width at 180 nm height. The light gray lines are the modes corresponding to the lowest vertical mode, and the dark lines at the bottom of (b) and (d) correspond to the second lowest vertical mode. The broken line indicates the height chosen for this design (180 nm). The family of second lowest vertical modes starts little after 180 nm, and as a consequence, the waveguides remain vertically single moded for the 1 μm to 5 μm range.
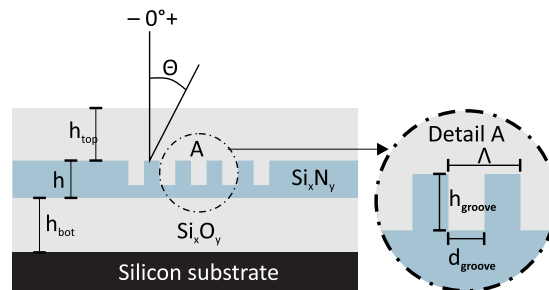

Fig. 3. Waveguide and grating schematic design. θ is the coupling angle measured with respect to the vertical. h_{top} is the top cladding height. h is the height of the waveguide core. h_{bot} is height of the bottom cladding. Detail A shows the grating period (Λ), the height of the groove (h_{groove}), and the width of the groove (d_{groove}).

of the receiving optical fiber and the out-coupling angle should coincide with the angle at which the optical fiber is installed [see Fig. 4(a)]. In an optogenetic device, however, light should be radiated out of the waveguide into a medium that contains cells (neurons). Neuron activation depends mainly on the power density of the emitted light regardless of the profile and the angle. Therefore, a grating coupler for optogenetics should be optimized such that most of the optical power carried by the waveguide is delivered to these neurons. Moreover, the power should be extracted within an area not larger than a cell body (10 μm to 20 μm; see Fig. 4(b)), and therefore, only one or very few neurons would be illuminated (i.e., single cell resolution).
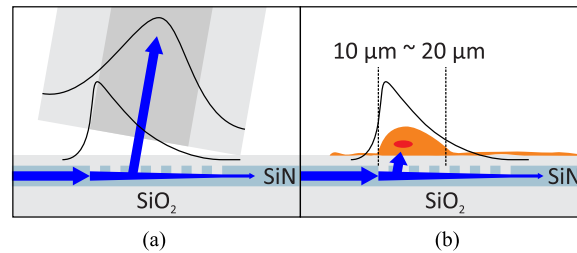
Fig. 4. Telecom versus optogenetic applications. (a) Grating coupler system to couple light into a single mode optical fiber. In this case, the output beam intensity profile has to be engineered to match as close as possible the Gaussian profile of the optical fiber. (b) System to deliver light to an optogenetic enable neuron. The beam intensity profile should carry most of the power in an area not larger than the body of the cell.
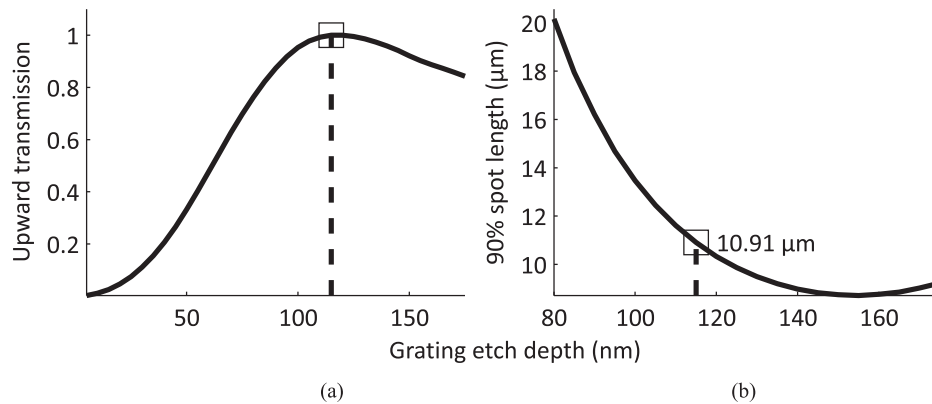

Fig. 5. (a) Normalized P_{up} versus h_{groove} for $\Lambda = 300$ nm and 30 grooves. (b) Extraction length for 90% of the power versus h_{groove}. The square mark shows a grating coupler depth of 115 nm and 90% extraction length of 10.91 μm.

For a uniform grating coupler, all grooves having the same shape, the profile of the emitted beam decays exponentially across the grating coupler. The decay length of this profile, and consequently the spot size, strongly depends on h_{groove}, where a deeper groove results in a shorter decay length. Furthermore, this parameter also determines the total amount of power directed upwards (towards the tissue). Therefore, h_{groove} should be selected such that the upward power (P_{up}) is maximized while the extraction length (the length at which 90% of the power has decayed) is kept within the specified dimensions (the size of a neuron). The height of the groove was found with a FEM model of the grating coupler with the already set parameters ($\Lambda = 300$ nm) and ($d_{groove} = 0.5*\Lambda$) and 30 periods, and it was simulated with the COMSOL 2D ewfd module. With this simulation the extraction length and P_{up} have been calculated with respect to h_{groove} (see Fig. 5). Consequently, an etch depth of 115 nm was selected since the corresponding P_{up} is close to the maximum and the extraction length (10.91 μm) complies to the neuron size requirement.

2.3 Fabrication Process

The PICs were fabricated on a 200 mm silicon wafer following a process that ensures CMOS back end compatibility. First, 2 μm of Si_xO_y were deposited using a high density plasma chemical vapor deposition (HDPCVD) process. Subsequently, the core layer (180 nm of Si_xN_y) was added using plasma-enhanced chemical vapor deposition (PECVD). The grating couplers were patterned using 193 nm optical lithography and a partial etch (115 nm) using an inductive coupled plasma reactive ion etch process based on fluorine etch chemistry. Subsequently, the waveguide cores were
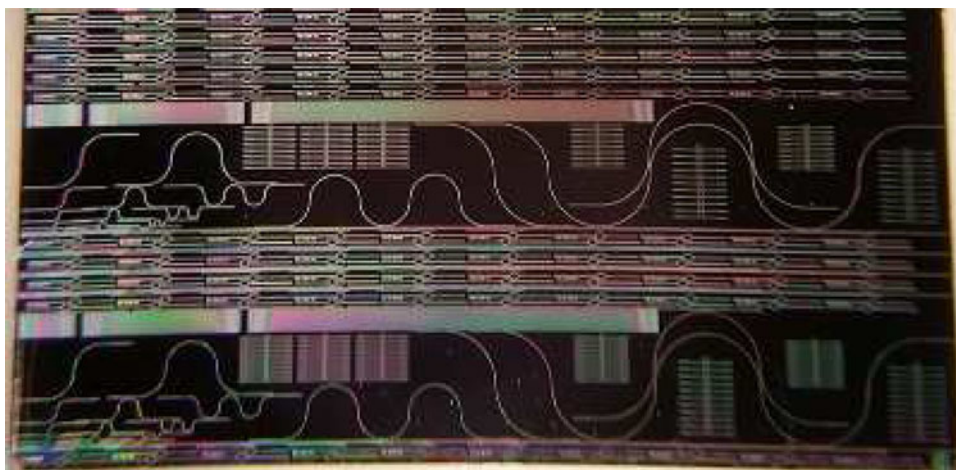
Fig. 6. Example of a complete processed chip. Silver color lines are the Si_xN_y waveguide test structures embedded in Si_xO_y.

formed by etching the Si_xN_y all the way to the bottom Si_xO_y layer, using the same process as the grating couplers. Finally, a second 2 μm layer of Si_xO_y was deposited as top cladding. For complete details on the fabrication process, see [6]. Fig. 6 shows a picture of the completely processed die.

3 Results

3.1 Test Chip

A test chip has been fabricated following the design of section 2.1. The layout included a range of straight waveguides of different lengths (1 mm to 16.9 mm) and widths (1 μm to 5 μm), as well as waveguides bends of different radii (25 μm to 1000 μm) for two different widths (1 μm and 5 μm). Grating couplers of 30 periods and 5 μm wide were positioned on each side of all the structures. Between these grating couplers and each PIC, tapers of 0.5 mm were placed that narrowed the waveguide to the corresponding width. Additionally, short straight waveguides of identical length with grating couplers of different number of grooves were also foreseen to measure the grating coupler decay length.

3.2 Measuring Setup

The characterization setup (see Fig. 7) incorporates a miniature laser diode of 450 nm (Osram, PL450B), which is a good candidate light source to be incorporated into an optogenetic device. The laser diode is powered by a precision current source (Keithley, 6221) Each input grating coupler is illuminated by placing the laser diode on top with a motorized micro-manipulator. As mentioned before, neuron activation by an output grating coupler only depends on the intensity of the emitted light and not on the direction or profile shape. Therefore, a 100 μm core optical fiber (Thorlabs, FG105ACA) was used to capture the outputted light, which better simulates this situation. The collected light power is measured by a photosensor (Thorlabs, S151C) connected to an optical power meter (Thorlabs, PM200), and the output fiber is positioned with a manual micro-manipulator.

Another version of the setup replaced the laser diode with a single mode optical fiber (Thorlabs, S405-XP) coupled to a laser diode (Thorlabs, LP450-SF15). This version was used for reference measurements and to measure the bend insertion losses. The cleaved tip of the fiber was positioned directly on top of the input grating coupler with the same motorized micro-manipulator. The angle and polarization of the input fiber were controlled with a goniometer and a fiber rotator respectively. The light at the out-coupling grating was still collected with the same multimode optical fiber.
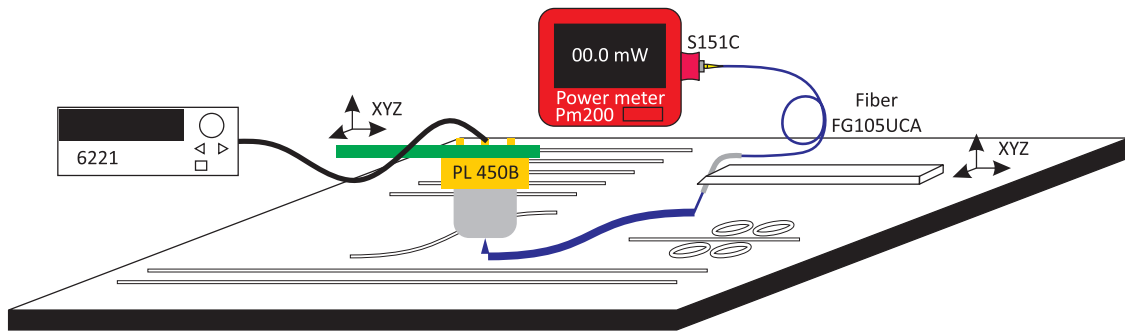
Fig. 7. Measuring setup. Each input coupler was illuminated by placing a laser diode (Osram, PL450B) on top of it with a motorized micro-manipulator. The light emitted by the output couplers was collected by a 100 μm core optical fiber (Thorlabs, FG105ACA) and measured by a photosensor (Thorlabs, S151C) connected to an optical power meter (Thorlabs, PM200). The optical fiber was placed on top of the output coupler with the help of a manual micro-manipulator. An alternative setup replaced the laser diode with a single mode optical fiber coupled to a laser diode.
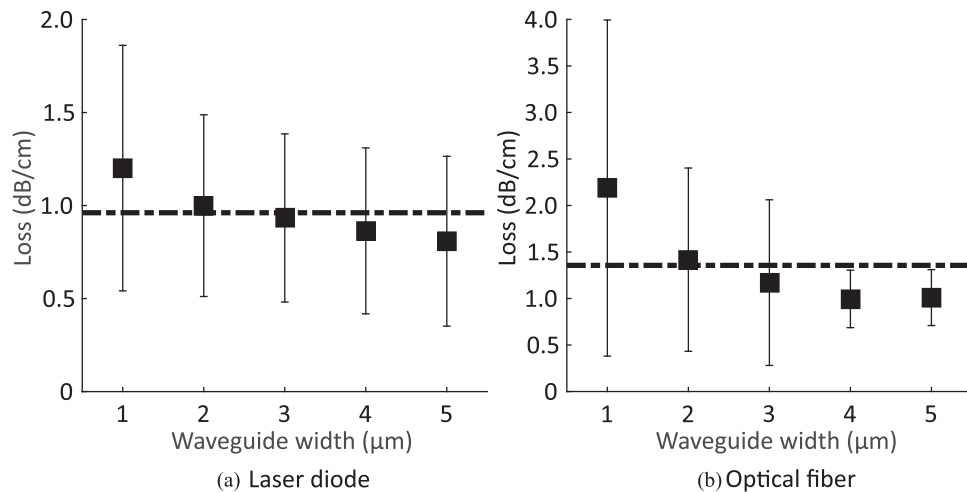

(a) Laser diode

(b) Optical fiber

Fig. 8. Propagation losses for Si_xN_y waveguides of different widths, excited by (a) miniature laser diode and (b) single mode optical fiber. The dotted line represents the mean of all losses. The error bar is the standard error. The number of chip samples was three.

3.3 Straight Waveguides Propagation Losses and Efficiency

The propagation losses were obtained for the straight waveguides using both the miniature laser diode and the optical fiber setups. This was achieved with waveguides of different lengths that were excited and their output power recorded (similar to the cut back method). This data was fitted to a decaying exponential ($P = Ae^{\alpha X}$). X corresponds to the length of the waveguide and the loss in dB/cm is extracted from the 'α' parameter using

$$L_{dB} = 10 \times \alpha \times \log(e). \tag{2}$$

Fig. 8 shows the measured losses for waveguides of different widths. For both measuring conditions, the propagation losses slightly decreased for wider waveguides. This behavior is characteristic of higher scattering losses caused by sidewall roughness and agrees with the observations from previous work that used the same Si_xN_y technology [6]. The average propagation losses were 1.23 $\pm$ 0.7 dB/cm for the optical fiber and 0.96 $\pm$ 0.4 dB/cm for the laser diode, which are very close to each other and very similar to those reported in [1]. In their study, Gorin *et al.* showed losses for
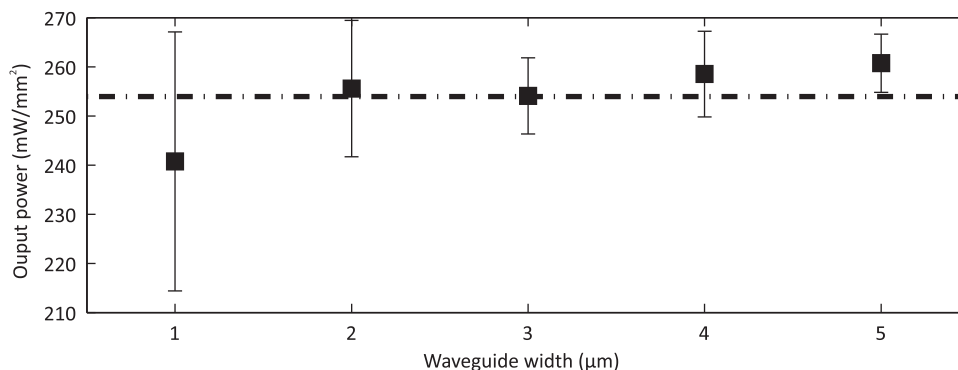
Fig. 9. Output power density of the longest waveguides of each width while excited by the miniature laser diode driven at its maximum power (~70 mW). The dotted line represents the mean. The error bars represent the standard error. The number of chip samples is 3.
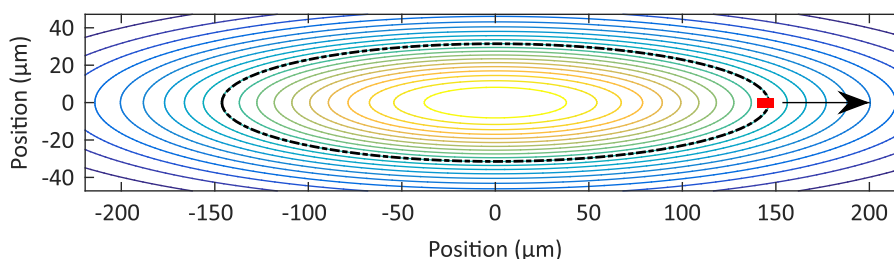

Fig. 10. Beam profile from the miniature laser diode at a distance of 900 μm on top of a grating coupler. The dashed line is the minimum nominal FWHM (full width half maximum) of the projected beam expected at this distance. The axis aspect ratio is one-to-one. The red rectangle represents the grating coupler and is on scale with the profile. The location of the grating coupler corresponds to the optimal position where the maximum coupling efficiency would be achieved given the incoming angle and power.

planar waveguides at 473 nm of 0.5 dB/cm for a refractive index of 1.89 and 1.04 dB/cm for one of 1.96. Their dataset can be extrapolated to obtain a rough loss estimation of 0.9 dB/cm at 450 nm which is very close to the values measured in the current study. Furthermore, they were also lower than the losses in [12], which were just below 3 dB/cm at 473 nm for a waveguide fabricated with LPCVD. This fabrication process is expected to have low losses, but their waveguides probably experienced high side wall roughness because they were patterned with (e-beam) lithography.

Also, it is very important to determine if the waveguides captured and transported enough light from the miniature laser diode to the output coupler so that the emitted power is sufficient for optogenetic applications. Fig. 9 shows the output power density of the longest waveguides (17.9 mm) of each width while excited with the miniature laser diode driven at its maximum power (~70 mW).

For all the widths, the power density was more than sufficient for the excitation of optogenetic transfected neurons (at least 1 mW/mm^2 [21]). The selected waveguide length is a good benchmark since the longest optogenetic devices to be manufactured would have waveguides of similar length. However, the total output power was only 12 μW which is about 0.02% of the input power and was lost mainly at the input grating. Very little light was coupled from the miniature laser diode because of the large distance between the emission point and the grating coupler (900 μm). This caused the beam to expand to a full width half maximum of at least 63 μm by 293 μm, which is considerably larger than the 5 μm by 10 μm coupler (see Fig. 10) and greatly reduced the power that reached the grating.

Fig. 10 shows that the power is the largest directly below the laser diode in the center of its profile, where the light propagates at an angle of 0°. Nevertheless, this angle would yield a very low coupling efficiency because the grating coupler design is optimized for light traveling at an
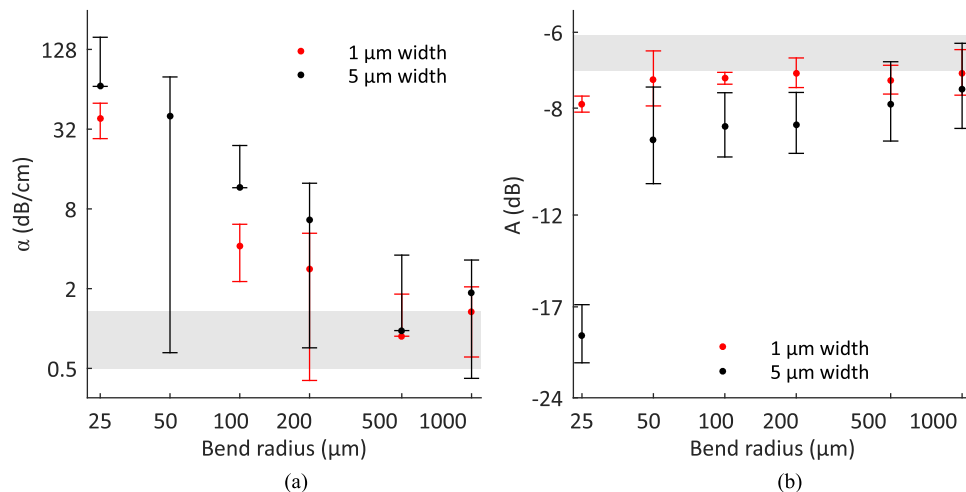
Fig. 11. (a) "α" parameter in function of bend radius obtained from fitting the data to a decaying exponential [see Eq. (3)]. The error bars are the confidence intervals of the fit. The lower bars are omitted when they fall below zero. The gray rectangle at the bottom corresponds to the straight waveguide propagation losses previously measured (see Fig. 8). The height of the bottom gray bar represents the corresponding error. (b) "A" parameter in function of bed radius obtained from fitting the data to a decaying exponential [see Eq. (3)]. The error bars are the confidence intervals of the fit. The gray rectangle at the top corresponds to the system efficiency obtained from the straight waveguides (see Fig. 8). The height of the rectangle represents the corresponding error. Data obtained from two chips.

angle of about 10° with respect to the vertical. The optimum angle can be reached by placing the grating (the laser diode in reality) away from the center of the beam in the direction parallel to the waveguide. However, displacing it too far would reduce the total incoming power, and therefore, the in-coupled power because of the beam's Gaussian distribution. Consequently, the grating position has to be optimized between these two extremes. The in-coupling efficiency in function of impinging angles was obtained with a FEM model of the grating coupler, which was solved with COMSOL's ewfd module. The total power at different positions (and therefore angles) was calculated from the beam profile. Putting these two together yields a theoretical coupling efficiency between 32.4 dB to 36.9 dB (0.06% to 0.02%), which is very close to the measured values. The range corresponds to the minimum and maximum nominal diverging angles, respectively, which has a direct effect on the power density of the distribution.

3.4 Bend Insertion Losses

For waveguide bends, there are three different mechanisms that contribute to the overall insertion losses [22]: mode mismatch at the transition between straight and bent sections, intrinsic bend losses due to "leaky" modes and waveguide propagation losses (same origin as for the straight waveguides). The bend insertion losses were measured only with the optical fiber setup in a similar way as with the straight waveguides. In this case, the output power from bends of the same radius but a different number of turns was collected and fitted to a decaying exponential in function of the number of turns "n":

$$P_{out} = A\, e^{-\alpha \times n \frac{\pi}{2} R}. \tag{3}$$

The decay parameter (α) includes the losses due to leaky modes, bend-to-bend transitions and straight propagation losses. The factor multipliying the exponential (A) includes the straight-to-bend transition losses and the bend-to-straight transition losses, which are negligible in a waveguide with large number of modes [23]. The "A" parameter also includes also the system coupling efficiency, which was obtained during the straight waveguide measurements.
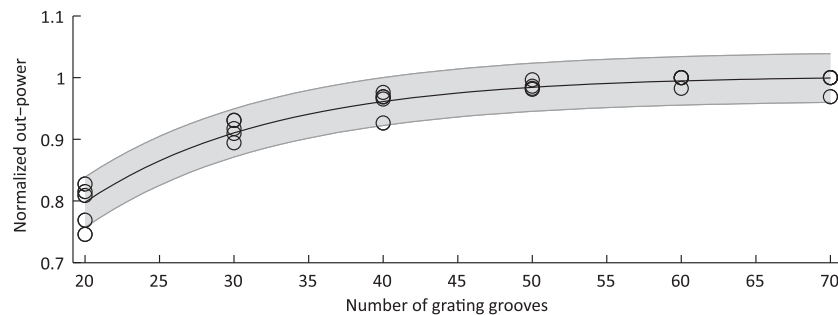
Fig. 12. Accumulated out-coupled light power for calculation of the out coupling length. The centerline represents the fitted result using $P_{out} = (1 - e^{(1/d)x})$, and the grayed area corresponds to the confidence interval of the predicted values by the fit. The number of samples per data point is five. Since the power has been normalized, some points fall in the same spot.

Fig. 11(a) presents the "α" parameter (i.e. the bend propagation losses) in function of the bend radius. It shows that the losses are lower for larger radii and that they are lower for the 1 μm wide bends than for the 5 μm ones. The difference between the two widths is explained by the fact that the higher order "leaky" modes are lossier in wider waveguides because their modes are closer to the critical angle. The same tendency is observed for the transition losses (i.e. parameter "A") [see Fig. 11(b)]. In this case, the behavior is explained by the large mode mismatch that occurs between a small radius bend and a straight waveguide, which is even bigger as the waveguide becomes wider.

The parameter "α" is compensated by subtracting the average straight propagation losses for the optical fiber setup obtained in Section 3.3. This results in the losses caused only by the bends. The compensated value is then multiplied by the corresponding arc length ($\frac{\pi}{2}$R) to obtain the losses per 90° turn. The lowest compensated losses were obtained for the 1 μm wide waveguides of 100 μm radius and corresponded to 45 × 10^{-3} dB. Similarly, the "A" parameter was compensated by subtracting the coupling efficiency from the straight waveguide measurements obtained in Section 3.3 in order to obtain the straight-to-bend transition losses. For the same 1 μm wide and 100 μm radius waveguide, the transition losses were 0.2 dB (about 5% loss). Both the losses and the radius are acceptable to allow fabrication of devices with good integration levels.

3.5 Grating Decay Length

Fig. 12 shows the normalized output power (P$_{out}$) as a function of the number of grating coupler grooves obtained by exciting gratings of a different number of periods. From this data, the decay length can be calculated by fitting it to $P_{out} = (1 - e^{(1/d)x})$, where '$d$' represents the decay length. This calculation yielded a decay length of 3.78 ± 0.76 μm, which implies that a little more than 90% of the power is outputted within the 30 grooves (9 μm) of the normal gratings. This result is in good agreement with the simulated spot size from Fig. 5 (~10 μm) and demonstrates that enough power can be delivered in a sufficiently small spot for single cell optogenetic stimulation.

4. Conclusion

Grating couplers and waveguides for blue light at 450 nm were fabricated and tested. The measured losses are in the order of 1 dB/cm for a width range from 1 μm to 5 μm. This value compares well to those obtained by [1] for un-patterned planar waveguides manufactured with PECVD and by [12] for LPCVD waveguides. The obtained bend losses were also reasonably low with a total transition loss of 0.2 dB/90° (5%) for a width of 1 μm and a radius of 100 μm, which is small enough to fabricate devices with good integration levels. Waveguides from all widths successfully coupled light from an un-collimated light source. The output power density for the longest 1 μm wide waveguide was about 240 mW/mm^2 with a spot size of 5 × 9 μm^2, which should allow single cell optical stimulation, and therefore, very high precision neuron interaction through optogenetics.

The obtained results offer better understanding of the behavior of Si_xN_y at blue wavelengths, its limitations and most importantly, what can be achieved with it in future. They demonstrate, for example, that a large number of optical outputs could be fabricated in a narrow shank because waveguides as narrow as 1 μm can be incorporated without significant loss of output power. Finally, all this confirms that the presented Si_xN_y platform is an excellent option for the manufacturing of optogenetic devices.

Acknowledgment

References

[1] A. Gorin, A. Jaouad, E. Grondin, V. Aimez, and P. Charette, "Fabrication of silicon nitride waveguides for visible-light using PECVD: A study of the effect of plasma frequency on optical properties," *Opt. Exp.*, vol. 16, no. 18, pp. 13 509–13 516, 2008.

[2] O. P. Parida and N. Bhat, "Characterization of optical properties of SU-8 and fabrication of optical components," *ICOP 2009-International Conf. Opt. Photonics CSIO*, p. PS3. E.8., 2009.

[3] A. N. Zorzos, E. S. Boyden, and C. G. Fonstad, "Multiwaveguide implantable probe for light delivery to sets of distributed brain targets," *Opt. Lett.*, vol. 35, no. 24, pp. 4133–4135, Dec. 2010. [Online]. Available: https://www.osapublishing.org/abstract.cfm?URI=ol-35-24-4133

[4] M. N. Polyanskiy, "Refractive index database." [Online]. Available: http://refractiveindex.info

[5] N. Daldosso *et al.*, "Comparison among various Si_3N _4 waveguide geometries grown within a CMOS fabrication pilot line," *J. Lightw. Technol.*, vol. 22, no. 7, pp. 1734–1740, Jul. 2004. [Online]. Available: http://dx.doi.org/10.1109/JLT.2004.831182

[6] A. Z. Subramanian *et al.*, "Low-loss singlemode PECVD silicon nitride photonic wire waveguides for 532–900 nm wavelength window fabricated within a CMOS pilot line," *IEEE Photon. J.*, vol. 5, no. 6, Dec. 2013, Art. no. 2202809.

[7] S. Romero-García, F. Merget, F. Zhong, H. Finkelstein, and J. Witzens, "Silicon nitride CMOS-compatible platform for integrated photonics applications at visible wavelengths," *Opt. Exp.*, vol. 21, no. 12, pp. 14 036–14046, 2013. [Online]. Available: http://www.opticsexpress.org/abstract.cfm?URI=oe-21-12-14036

[8] K. Deisseroth, "Controlling the brain with light," *Sci. Amer.*, vol. 303, no. 5, pp. 48–55, 2010.

[9] F. Zhang, L.-P. Wang, E. S. Boyden, and K. Deisseroth, "Channelrhodopsin-2 and optical control of excitable cells," *Nature Methods*, vol. 3, no. 10, pp. 785–792, 2006. [Online]. Available: http://www.ncbi.nlm.nih.gov/pubmed/16990810

[10] J. Tauc, "Optical properties and electronic structure of amorphous Ge and Si," *Mater. Res. Bull.*, vol. 3, no. 1, pp. 37–46, 1968. [Online]. Available: http://linkinghub.elsevier.com/retrieve/pii/0025540868900238

[11] E. Segev, T. Fowler, A. Faraon, and M. L. Roukes, "Visible array waveguide gratings for applications of optical neural probes," *Proc. SPIE*, vol. 9305, Mar. 2015, Art. no. 93052L. [Online]. Available: http://proceedings.spiedigitallibrary.org/proceeding.aspx?doi=10.1117/12.2078599

[12] E. Shim, Y. Chen, S. Masmanidis, and M. Li, "Multisite silicon neural probes with integrated silicon nitride waveguides and gratings for optogenetic applications," *Sci. Rep.*, vol. 6, Mar. 2016, Art. no. 22693. [Online]. Available: http://www.nature.com/articles/srep22693

[13] L. Hoffman *et al.*, "High-density optrode-electrode neural probe using Si_xN_y photonics for in vivo optogenetics," in *Proc.IEEE Int. Electron Devices Meet.*, Dec. 2015, pp. 29.5.1–29.5.4. [Online]. Available: http://ieeexplore.ieee.org/lpdocs/epic03/wrapper.htm?arnumber=7409795

[14] M. Welkenhuysen *et al.*, "An integrated multi-electrode-optrode array for in vitro optogenetics," *Sci. Rep.*, vol. 6, Feb. 2016, Art. no. 20353. [Online]. Available: http://www.nature.com/articles/srep20353

[15] S. Musa *et al.*, "Planar 2D-array neural probe for deep brain stimulation and recording (DBSR)," in *Proc. Int. Fed. Med. Biol. Eng.*, 2002, vol. 22, pp. 2421–2425. [Online]. Available: http://link.springer.com/10.1007/978-3-540-89208-3_581

[16] C. M. Lopez *et al.*, "An implantable 455-active-electrode 52-channel CMOS neural probe," *IEEE J. Solid-State Circuits*, vol. 49, no. 1, pp. 248–261, Jan. 2014.

[17] R. G. Hunsperger, *Integrated Optics: Theory and Technology*. Berlin, Germany: Springer-Verlag, 2009. [Online]. Available: http://link.springer.com.sci-hub.org/content/pdf/10.1007/b98730.pdf

[18] A. Z. Subramanian, S. Selvaraja, P. Verheyen, A. Dhakal, K. Komorowska, and R. Baets, "Near-infrared grating couplers for silicon nitride photonic wires," *IEEE Photon. Technol. Lett.*, vol. 24, no. 1, pp. 1700–1703, Oct. 2012.

[19] G. Maire *et al.*, "High efficiency silicon nitride surface grating couplers," *Opt. Exp.*, vol. 16, no. 1, pp. 328–333, 2008.

[20] T. Tamir and S. T. Peng, "Analysis and design of grating couplers," *Appl. Phys.*, vol. 14, no. 3, pp. 235–254, 1977.

[21] E. S. Boyden, F. Zhang, E. Bamberg, G. Nagel, and K. Deisseroth, "Millisecond-timescale, genetically targeted optical control of neural activity," *Nature Neurosci.*, vol. 8, no. 9, pp. 1263–1268, 2005. [Online]. Available: http://www.ncbi.nlm.nih.gov/pubmed/16116447

[22] I. Papakonstantinou, K. Wang, D. R. Selviah, and F. A. Fernández, "Transition, radiation and propagation loss in polymer multimode waveguide bends," *Opt. Exp.*, vol. 15, no. 2, pp. 669–679, Jan. 2007. [Online]. Available: https://www.osapublishing.org/oe/abstract.cfm?uri=oe-15-2-669

[23] I. Salinas, I. Garcés, R. Alonso, A. Llobera, and C. Domínguez, "Simple estimation of transition losses in bends of wide optical waveguides by a ray tracing method," *IEEE Photon. Technol. Lett.*, vol. 16, no. 3, pp. 825–827, Mar. 2004.